LAWRENCE
LIVERMORE
NATIONAL
LABORATORY

LLNL-JRNL-407462

First Principles Molecular Dynamics Investigation of Bulk and Interfacial Aqueous Fluoride

M.-H. Ho, I-F. W. Kuo, M. L. Klein

October 3, 2008

Journal of Physical Chemistry A

Disclaimer

First Principles Molecular Dynamics Investigation of Bulk and Interfacial Aqueous Fluoride

Ming-Hsun Ho,[1] I-F. William Kuo,[2] and Michael L. Klein[1]*

[1]Department of Chemistry and Center for Molecular Modeling, University of Pennsylvania

Philadelphia, Pennsylvania 19104-6323

[2]Chemical Sciences Division, Lawrence Livermore National Laboratory

P.O. Box 808, Livermore, CA 94551

RECEIVED DATE: September 30, 2008

* E-mail: kuo2@llnl.gov

ABSTRACT

Using first principles molecular dynamics simulation, we have embedded a fluoride anion into a water slab composed of 215 water molecules to mimic bulk and interfacial solvation. Our findings indicate that there are small structural changes for fluoride and its first solvation shell but the presence of fluoride does not alter the rotational dynamics of nearby water. In addition, we have computed the molecular dipole moments using Wannier centers. At the interface, the presence of fluoride increases the molecular dipole moments of nearby water molecule, whereas in the bulk the molecular dipole moments for water appears to be invariant to the presence of fluoride in the vicinity. Previous study of the air-water interface shows water at the interface have higher average HOMO energies and thus more prone to electrophilic attack. With the addition of fluoride, the most likely reactive site for electrophilic reactions shifts to the anion. This could explain the large increase in reaction rates for heterogeneous process. The reactive properties of other anions near the GDS are of great interest in heterogeneous chemistry and can be elucidated using the same type of analysis performed here for fluoride anion.

KEYWORDS: air-water, liquid-vapor, interface, fluoride, and halides.

I. Introduction:

Hydrogen bonding fluids are associated to many important process in natural sciences have been studied extensively using molecular simulations. In particular, the resurgence of interests in the study of surface properties of electrolyte solutions at the liquid-vapor interfaces has been enhanced due to recent experiments and theoretical studies.[1-16] Counter to the previous notion that the air-water interface is deplete of alkali halide ions, recent experiments are showing population enhancements at the liquid-vapor interface. In addition, recent theoretical studies using classical polarizable potentials have elucidated the effect of ion size and polarizability on increase surface enhancements at the liquid-vapor interface. The ramification of this increase in alkali halide ions at the liquid-vapor interface is profound where heterogeneous chemistry is taken into account.[17,18] In comparison to our understanding of the structural and dynamical properties of electrolytic solutions at the liquid-vapor interface, electronic properties and chemical reactivity due to the presence of the alkali halide ions is relatively unknown and is an area ripe for further investigation. One method to gain insight into chemical reactivity is to utilize electronic structure calculation where ions are solvated in water cluster.[15,16] Although insights can be gleaned by using a water cluster approach, it can not compensate for the anisotropic solvation of a true interface. This effect will become even more important with increasing size or polarizability of the solvated ions and thus its chemical reactivity. In this study, we will look at the effective change in structure, dynamics, and chemical reactivity at the interface in the presence of an anion using a water slab.

With recent advances in fast electronic structure algorithms and high-performance computing, it is now common to perform neat liquid-vapor interface simulations using first principles molecular dynamics simulation utilizing density functional theory (DFT) based interaction potentials.[19-21] Prior studies have shown that DFT using gradient corrected functionals such as Becke-Lee-Yang-Parr (BLYP)[22,23] exchange and correlation functional can reproduce experimental measurements for most aqueous system including surface sensitive experiments. One glaring problem with the use of DFT based interaction potentials is the failure to correctly predict the density of hydrogen bonded fluids possibility due to the lack of London dispersion forces in DFT. In addition, it has been shown that first principles molecular dynamics simulations are capable of qualitatively reproducing potential of mean force curves for model electrolytic systems.[4] In this study, we will look at the effective change in structure, dynamics, and chemical reactivity at the liquid-vapor interface of a model electrolyte solution. We have chosen to simulate the effect of one fluoride anion on the structure, dynamics, and electronic property at the air-water interface, due to the high computational of sampling even on the picosecond time scale.

II. Simulation Details:

First principles molecular dynamics simulations within the Born-Oppenheimer approximation were performed using the software suite CP2K where the energy and force was obtained from the QuickStep module. [24,25] The QuickStep module contain a fast electronic structure code based on the Kohn-Sham (KS) formulation of DFT.[26] For these calculations, a dual basis set of Gaussian type orbitals (TZV2P) with auxiliary plane waves expanded up to 280 Ry were utilized to describe the valence states. The core states are described through the Goedecker-Teter-Hutter pseudopotential.[27] These combination of basis sets and pseudopotentials has been validated to give converged properties for aqueous system.[25] The calculations were performed using the BLYP[22,23] exchange and correlation functionals due to its ubiquitous use in studies of aqueous system. Simulations were carried out in the canonical ensemble using a timestep of 0.48 fs. Nosé-Hoover chain[28-30] thermostats of length 3 were attached to every degree of freedom, with a time constant of 100 fs to ensure thermal equilibrium at 300 K over the entire simulation trajectory.

Five independent first principles molecular dynamics simulations were performed using the slab configuration. Unlike previous liquid-vapor interface simulations, the simulations for this study contains 215 water molecules plus one fluoride anion in a simulation cell of dimension 15 Å x 15 Å x 71.44 Å. Embedding only one fluoride anion versus a high concentration of fluoride anions was chosen to clearly differentiate the changes to surface property due to the presence of the ion using a finite amount of computational resources. The size of the simulation cell in the *z* direction was chosen to ensure the decoupling of the two interfaces.[31] In each of the five simulations, fluoride was constraint to be at different interfacial depth of 0.0 Å, 1.06 Å, 2.12 Å, 16.93 Å, and 17.99 Å as measured from the center of the water slab. These depths were chosen to adequately sample the fluoride anion at two main target locations namely the bulk region (0.0 Å, 1.06 Å, and 2.12 Å) as well as near the Gibbs dividing surface (16.93 Å and 17.99 Å). For simplicity, we will refer to the two groups of simulation as SET_A and SET_B for fluoride solvated in the bulk region of the water slab and fluoride near the Gibbs dividing surface respectively from this point forward. Each simulation consists of 2 ps equilibration and a production run of 6 ps except for the 17.99 Å simulation where 12 ps of production run was used in the data analysis.

III. Results and Discussion:

Density Profile

Large fluctuations in the density along the *z*-axis is usually an early indicator of an unstable interfacial

slab. Density profiles are shown in Figure 1. The density of the interfacial slab along the z-axis was tabulated using 1 Å wide bins. A best-fit density profile using a hyperbolic tangent function of the form:

$$\rho(z) = \frac{1}{2}(\rho_l + \rho_v) - \frac{1}{2}(\rho_l - \rho_v)\tanh\left(\frac{z - z_{GDS}}{\delta}\right) \quad \text{Eqn. 1}$$

are also shown. Here ρ_l and ρ_v correspond to liquid and gas density, z_{GDS} is the Gibbs dividing surface, and δ is an interface thickness parameter. This same procedure has been used previously to characterize the neat air-water interface using DFT interaction potential.[20] To improve statistics, the 5 simulations have been grouped into SET_A and SET_B as described above. Due to the simulated timescale and finite size of our system, ρ_v was set to be zero explicitly in the fitting as no evaporation is observed. The resulting best-fit parameters are shown in Table 1. Both Figure 1 and the fitted parameter ρ_l for both SET_A and SET_B shows the interfacial slab, have a low predicted density of 0.8 g/cm^3 in the bulk region when compared to experimental density. The small difference in liquid density (ρ_l) between SET_A and SET_B are within the statistical noise. This again reconfirms prior results of low predicted density for aqueous system obtained with different simulation codes, sampling methods, and ensembles.[19,32,33] Although the interfacial thickness parameter, δ, is highly sensitive to the fitting procedure, the interfacial thickness for SET_A, 0.836 Å, is comparable to the value of 0.786 Å obtained for neat air-water interface.[20] In the presence of ion near the GDS, a value of 1.547 Å was obtained for SET_B. This increased interfacial thickness in the presence of ions has also been observed previously.[34] Overall, there were no large fluctuations in the density profile, thus we believe that we have stable interfaces. In addition, we can estimate the thickness of our interfacial slab after equilibration as 2 x z_{GDS}. Thus for our simulations, the thickness are 35.0 Å and 35.5 Å for SET_A and SET_B respectively.

Radial distribution functions

The radial distribution function (RDF) for fluoride-oxygen and fluoride-hydrogen (i.e. $g_{FO}(r)$ and $g_{FH}(r)$ respectively) are shown in **Figure 2** for fluoride solvated in the bulk region and near the GDS. The computed coordination number is 4.1 for both fluorine-oxygen and fluorine-hydrogen for SET_A. These values are slightly different from the oxygen-oxygen and oxygen-hydrogen coordination number of liquid water thus indicating a slight perturbation of hydrogen bond network due to the presence of fluorine. In addition, the fluorine-oxygen and fluorine-hydrogen coordination number for SET_B are both 3.5. Overall, it was observed that fluorine is mostly bound to neighboring water in a tetrahedral geometry in contrast to previous observations of square pyramidal coordination structure also using DFT potential.[35] The difference in solvation structure is most likely due to the use of experimental density as well as a neutralizing background charge. Overall, the presence of fluoride results in a very

well defined first solvation peak around 2.6 Å and minimum around 3.3 Å for both sets of $g_{FO}(r)$. Likewise the $g_{FH}(r)$ RDF also shows very well defined first solvation peak around 1.6 Å and first minimum around 2.5 Å. It should be noted that for both $g_{FO}(r)$ and $g_{FH}(r)$, we did noticed a small decrease for the position of the first solvation peaks of 0.05 Å going from SET_A to SET_B. One interesting feature to note is the appearance of a small peak around 1.04 Å for $g_{FH}(r)$. This peak can be attributed to the fact that fluoride is the conjugate base of a weak acid and thus can form molecular hydrogen fluoride to account for the peak around 1.04 Å. The larger peak at 1.6 Å is due to the solvation of fluoride anion by neighboring water molecules and can partially explain for the slight peak shift observed going from bulk to surface. Distinct RDFs for solvated ion (F^-) versus solvated molecular hydrogen fluoride (HF) has been observed previously from first principles simulation.[36-38] Although an exhaustive discussion of published RDFs obtained using first principles simulations on fluoride containing aqueous solution is not constructive due to the different simulation protocol as well as system simulated,[35-38] it should be noted that there are important differences that can be gleaned. In addition, another prominent difference is the peak height of the first solvation shell for $g_{FO}(r)$ where we obtained a value of 5.5 which is closer to what was observed from neutron diffraction data[39] and simulations carried out by Heuft and Meijer[35] than results of Sillanpaa et. al.[36] The discrepancies between first principles simulation results can be due to the splitting of the first solvation peak resulting in a lower but wider first solvation structure. In addition, it should be noted that the use of experimental liquid density in prior studies versus the use of the slab geometry allows for the system to relax to its natural density and thus can also alter the RDFs.

Rotational Correlation

The time correlation function, $C_2(t)$, for molecular reorganization of water was computed according to

$$C_2(t-t_0) = \left\langle P_2\left[\vec{r}(t-t_0)\cdot\vec{r}(t_0);t\right]\right\rangle$$

where P_2 represents the second Legendre polynomial. The bisector for the H-O-H angle was chosen as the molecular vector $\vec{r}$. The water slab was partitioned into two group categorized as "bulk" or "surface" region using an imaginary plane located at 2δ below the GDS as the cutoff. The correlation function, $C_2(t)$, shown in Figure 3 allows for the comparison of dynamic properties of individual water as a function of location. The salient feature of this plot is that there is a clear difference between the time correlation functions for water in the bulk region versus surface region. Systematically, the rotational dynamics for water appears to be faster for surface region water than bulk region water. Similar behavior has been observed previously for air-water and air-methanol interfaces.[20,21] In addition, if the rotationally dynamics of water is altered due to hydrogen bonding to the fluoride anion, we would

expect $C_2(t)$ at the surface to change more dramatically then bulk region $C_2(t)$ simply because of the number of flouride-water/water-water hydrogen bond ratio is larger at the surface and thus larger signal to noise ratio. From Figure 3, there appears to be no effective change in the rotational dynamics of water at the surface for SET_B that could be resolved from our simulation trajectory. Likewise, there appears to be no changes to $C_2(t)$ for water in the bulk region with and without the presence of fluoride anion.

Molecular Dipoles

Molecular dipole moments for water and fluoride anion were computed via the Wannier centroid analysis where we assume each molecule/ion have four centers with electronic charge centers reflecting the nature of spin restricted calculation.[40,41] The average molecular dipole moment as a function of interfacial depth for water is shown in Figure 4. For both SET_A and SET_B, the average molecular dipole for water has the same qualitative behavior as observed for neat air-water interface where the average molecular dipole moments for water is around 3.0 D in the bulk region and decreases dramatically to a value around 2.0 D in the interfacial region.[19] This same qualitative trend has been seen in other liquid-vapor calculations using first principles simulations as well as polarizable empirical potentials.[20,21,42] From Figure 4, we conclude that the presence of fluoride in the bulk region has no direct influence on the molecular dipole of neighboring water since SET_A and SET_B appears indistinguishable. This observation was also noted in previous solvated aqueous fluoride simulations.[35,43] With the propensity for the molecular dipole moments of water to decrease going from bulk to interface and previous observation that fluoride does not perturb the electronic structure of neighboring water, it would be expected that SET_A and SET_B should be indistinguishable near the GDS. Unlike the bulk region, the presence of fluoride near the GDS (SET_B) shows an increase in both the average molecular dipole as well as a substantial increase in standard deviation. Since fluoride is still completely solvated near the GDS as described above, the increase in molecular dipole is caused by anisotropy of interface and not partial solvation of the first hydration shell as seen for ion-water clusters.[43] As a result, the systematic shift towards larger dipole moment for fluoride anion is expected and is shown in the inset of Figure 4.

Molecular States

By utilizing the method developed by Vuilleumier and Sprik[44], we have computed the effective highest occupied molecular orbital (HOMO) energies for each molecule (**Figure 5**). The effective HOMO energy distributions for fluoride in the bulk region and near the GDS are shown in the inset of **Figure 5**. For both air-water and air-methanol interface, it was found that the average HOMO energies

increases going toward the interface and thus paints a picture of a reactive surface susceptible to electrophilic attacks.[19,21] Surprisingly, with the addition of a fluoride ion, it was found that the average HOMO energies for water is relatively constant as a function of interfacial depth. More interestingly, the HOMO energy for fluoride shows a shift of 0.025H going from the bulk region to the surface region as seen in the inset of **Figure 5**. This shift makes the fluoride at the interface more susceptible to electrophilic attack than any other molecule and could explain why halides at the interface can dominate chemical reaction pathways.[17]

IV. Conclusions:

Using first principles molecular dynamics simulation, we have embedded fluoride anion into a water slab to mimic bulk and interfacial solvation. There are unanswered questions regarding the density of hydrogen-bonded fluids using DFT potential, thus the use of the slab geometry does ensures the simulations were carried out at the natural equilibrium density for the potential. In the bulk region, we observed tetrahedrally coordinated solvation structure around the fluoride in both bulk and surface region of the water slab. In addition, we also found small systematic shifts in the first solvation structure as seen in the RDF as well as a small but finite propensity to form molecular hydrogen fluoride at the interface. Although small structural differences were observed, the effect of fluoride on the rotational dynamics of neighboring water is minimal regardless of whether it's in the bulk region or surface region of the water slab. The most dramatic changes on interfacial properties are electronic in nature when the ion was present near the GDS. It was observed that the presence of fluoride near the GDS both increases and alters the molecular dipole moment distribution of neighboring water where such effects are not observed in the bulk region. As a result, the molecular dipole moment of fluoride anion also increases near the GDS due to increase polarization of neighboring water molecules. Furthermore, the presence of fluoride anion also alters the effective HOMO energies for water throughout the water slab. Unlike previous liquid-vapor interface where interfacial molecules have higher energies and thus more reactive in nature, the presence of fluoride in the water slab causes the potential reactive sites to be shifted to the anion. Whether this behavior is representative of other halides is of great interest and can be elucidated in the future by utilizing the same type of simulations and analysis performed here for fluoride anion.

ACKNOWLEDGMENT Part of this work was performed under the auspices of the U.S. Department of Energy by Lawrence Livermore National Laboratory under Contract DE-AC52-07NA27344. Computing resources was provided by Livermore Computing. We would like to thank LLNL

Computing staff for their help. MHH thank the National Institutes of Health (NIH) for their financial support.

REFERENCES

(1) Ghosal, S.; Hemminger, J. C.; Bluhm, H.; Mun, B. S.; Hebenstreit, E. L. D.; Ketteler, G.; Ogletree, D. F.; Requejo, F. G.; Salmeron, M. *Science* **2005**, *307*, 563.

(2) Otten, D. E.; Petersen, P. B.; Saykally, R. J. *Chem. Phys. Lett.* **2007**, *449*, 261.

(3) Uejio, J. S.; Schwartz, C. P.; Duffin, A. M.; Drisdell, W. S.; Cohen, R. C.; Saykally, R. J. *PNAS* **2008**, *105*, 6809.

(4) Brown, M. A.; D'Auria, R.; Kuo, I. F. W.; Krisch, M. J.; Starr, D. E.; Bluhm, H.; Tobias, D. J.; Hemminger, J. C. *Phys. Chem. Chem. Phys.* **2008**, *10*, 4778.

(5) Soule, M. C. K.; Blower, P. G.; Richmond, G. L. *J. Phys. Chem. B* **2007**, *111*, 13703.

(6) Soule, M. C. K.; Blower, P. G.; Richmond, G. L. *J. Phys. Chem. A* **2007**, *111*, 3349.

(7) Gopalakrishnan, S.; Jungwirth, P.; Tobias, D. J.; Allen, H. C. *J. Phys. Chem. B* **2005**, *109*, 8861.

(8) Xu, M.; Larentzos, J. P.; Roshdy, M.; Criscenti, L. J.; Allen, H. C. *Phys. Chem. Chem. Phys.* **2008**, *10*, 4793.

(9) Jungwirth, P.; Tobias, D. J. *J. Phys. Chem. B* **2002**, *106*, 6361.

(10) Jungwirth, P.; Tobias, D. J. *Chem. Rev.* **2006**, *106*, 1259.

(11) Tobias, D. J.; Hemminger, J. C. *Science* **2008**, *319*, 1197.

(12) Yu, Y.; Ezell, M. J.; Zelenyuk, A.; Imre, D.; Alexander, L.; Ortega, J.; Thomas, J. L.; Gogna, K.; Tobias, D. J.; D'Anna, B.; Harmon, C. W.; Johnson, S. N.; Finlayson-Pitts, B. J. *Phys. Chem. Chem. Phys.* **2008**, *10*, 3063.

(13) Jungwirth, P.; Winter, B. *Ann. Rev. Phys. Chem.* **2008**, *59*, 343.

(14) Wick, C. D.; Dang, L. X. *Chem. Phys. Lett.* **2008**, *458*, 1.

(15) Cwiklik, L.; Buck, U.; Kulig, W.; Kubisiak, P.; Jungwirth, P. *J. Chem. Phys.* **2008**, *128*, 154306.

(16) Frigato, T.; VandeVondele, J.; Schmidt, B.; Schutte, C.; Jungwirth, P. *J. Phys. Chem. A* **2008**, *112*, 6125.

(17) Knipping, E. M.; Lakin, M. J.; Foster, K. L.; Jungwirth, P.; Tobias, D. J.; Gerber, R. B.; Dabdub, D.; Finlayson-Pitts, B. J. *Science* **2000**, *288*, 301.

(18) Gard, E. E.; Kleeman, M. J.; Gross, D. S.; Hughes, L. S.; Allen, J. O.; Morrical, B. D.; Fergenson, D. P.; Dienes, T.; Galli, M. E.; Johnson, R. J.; Cass, G. R.; Prather, K. A. *Science* **1998**, *279*, 1184.

(19) Kuo, I. F. W.; Mundy, C. J. *Science* **2004**, *303*, 658.

(20) Kuo, I. F. W.; Mundy, C. J.; Eggimann, B. L.; McGrath, M. J.; Siepmann, J. I.; Chen, B.; Vieceli, J.; Tobias, D. J. *J. Phys. Chem. B* **2006**, *110*, 3738.

(21) Kuo, I. F. W.; Mundy, C. J.; McGrath, M. J.; Siepmann, J. I. *J. Phys. Chem. C* **2008**, *112*.

(22) Becke, A. D. *Phys. Rev. A* **1988**, *38*, 3098.

(23) Lee, C.; Yang, W.; Parr, R. G. *Phys. Rev. B* **1988**, *37*, 785.

(24) CP2K. http://cp2k.berlios.de.

(25) VandeVondele, J.; Krack, M.; Mohamed, F.; Parrinello, M.; Chassaing, T.; Hutter, R. *Comput. Phys. Commun.* **2005**, *167*, 103.

(26) Lippert, G.; Hutter, J.; Parrinello, M. *Mol. Phys.* **1997**, *92*, 477.

(27) Goedecker, S.; Teter, M.; Hutter, J. *Phys. Rev. B* **1996**, *54*, 1703.

(28) Hoover, W. G. *Phys. Rev. A* **1985**, *31*, 1695.

(29) Nose, S. *J. Chem. Phys.* **1984**, *81*, 511.

(30) Martyna, G. J.; Klein, M. L.; Tuckerman, M. *J. Chem. Phys.* **1992**, *97*, 2635.

(31) Mundy, C. J.; Kuo, I. F. W. *Chem. Rev.* **2006**, *106*, 1282.

(32) Kuo, I. F. W.; Mundy, C. J.; McGrath, M. J.; Siepmann, J. I.; VandeVondele, J.; Sprik, M.; Hutter, J.; Chen, B.; Klein, M. L.; Mohamed, F.; Krack, M.; Parrinello, M. *J. Phys. Chem. B* **2004**, *108*, 12990.

(33) Mcgrath, M. J.; Siepmann, J. I.; Kuo, I. F. W.; Mundy, C. J.; VandeVondele, J.; Hutter, J.; Mohamed, F.; Krack, M. *J. Phys. Chem. A* **2006**, *110*, 640.

(34) Warren, G. L.; Patel, S. *J. Phys. Chem. B* **2008**, *112*, 11679.

(35) Heuft, J. M.; Meijer, E. J. *J. Chem. Phys.* **2005**, *122*, 094501.

(36) Sillanpaa, A. J.; Simon, C.; Klein, M. L.; Laasonen, K. *J. Phys. Chem. B* **2002**, *106*, 11315.

(37) Simon, C.; Klein, M. L. *Chemphyschem* **2005**, *6*, 148.

(38) Laasonen, K.; Larrucea, J.; Sillapaa, A. *J. Phys. Chem. B* **2006**, *110*, 12699.

(39) Soper, A. K.; Weckstrom, K. *Biophys. Chem.* **2006**, *124*, 180.

(40) Berghold, G.; Mundy, C. J.; Romero, A. H.; Hutter, J.; Parrinello, M. *Phys. Rev. A* **2000**, *61*, 10040.

(41) Silvestrelli, P. L.; Parrinello, M. *Phys. Rev. Lett.* **1999**, *82*, 3308.

(42) Wick, C. D.; Kuo, I. F. W.; Mundy, C. J.; Dang, L. X. *J. Comput. Theo. Chem.* **2007**, *3*, 2002.

(43) Krekeler, C.; Hess, B.; Delle Site, L. *J. Chem. Phys.* **2006**, *125*, 054305.

(44) Vuilleumier, R.; Sprik, M. *J. Chem. Phys.* **2001**, *115*, 3454.

Table 1. Fitted density profile parameters for liquid-vapor interface with fluoride situated at different depth. The density profile was fitted using $\rho(z) = \frac{1}{2}(\rho_l + \rho_v) - \frac{1}{2}(\rho_l - \rho_v)\tanh\left(\frac{z - z_{GDS}}{\delta}\right)$ with the center of mass shifted to $z = 0$ Å for the fitting. A tabulation of all the fitted parameters from the simulations are also shown.

	ρ_l (g/cm^3)	δ (Å)	z_{GDS} (Å)
SET_A	0.799	0.836	17.49
SET_B	0.792	1.547	17.75

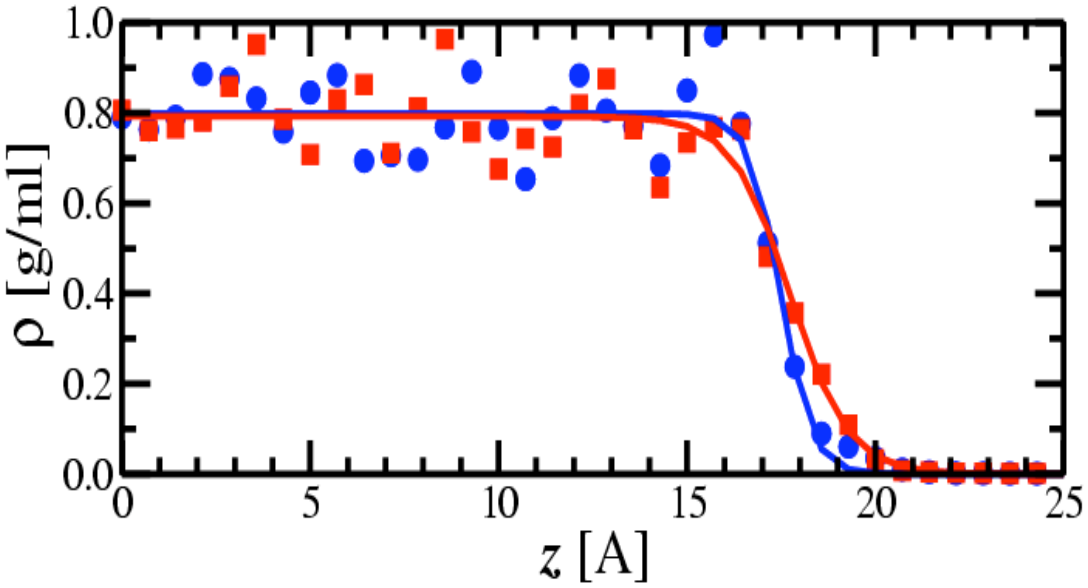

Figure 1. Density profiles for liquid-vapor slab with fluoride. The three simulations where the anions are in the bulk region (SET_A) are shown in *blue* and the two simulation representing fluoride near the GDS (SET_B) are shown in *red*. The GDS are located at 17.49 Å and 17.75 Å for SET_A and SET_B respectively.

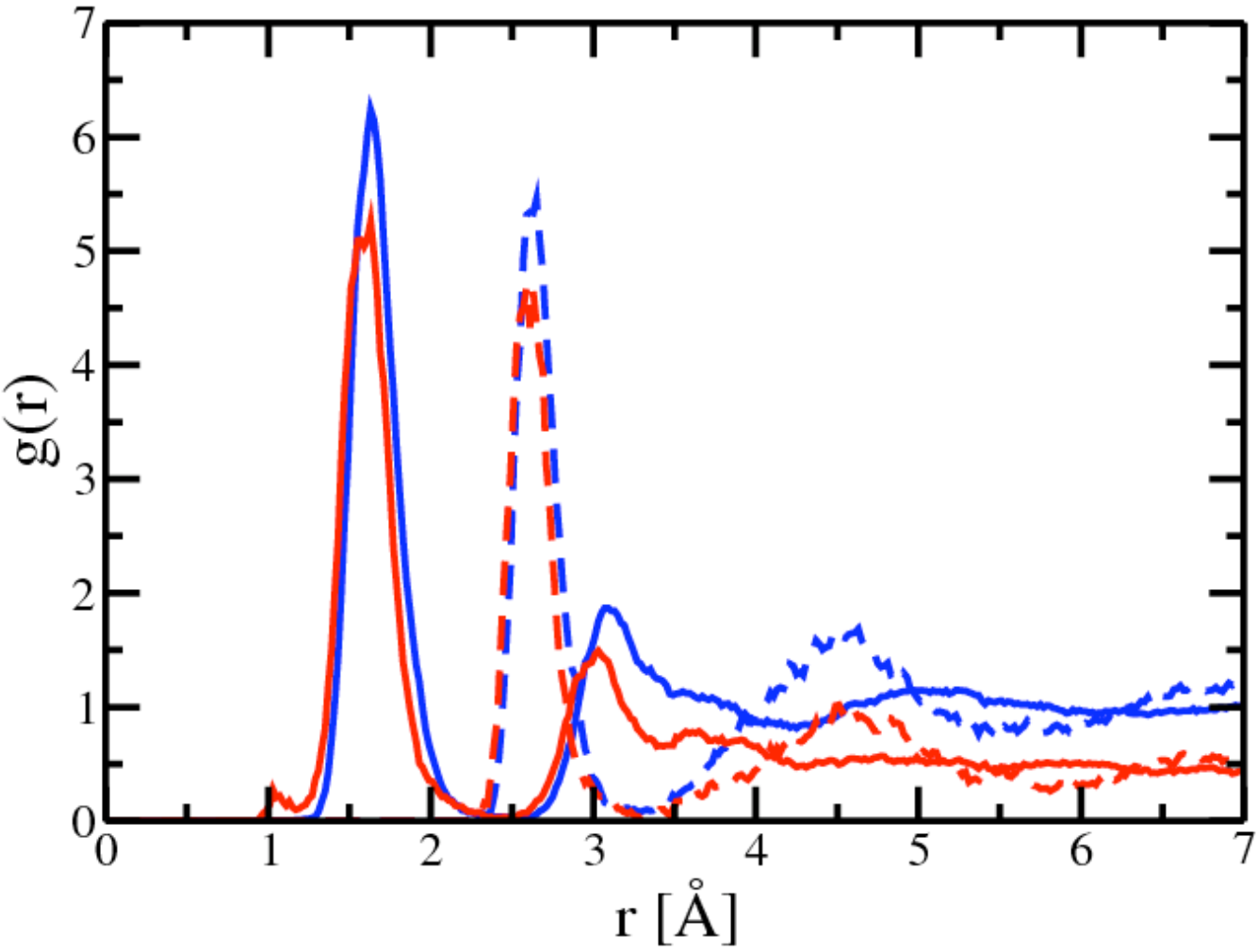

Figure 2. The radial distribution functions (RDF) for fluoride-oxygen ($g_{FO}(r)$) and fluoride-hydrogen ($g_{FH}(r)$)are shown with dash and solid lines respectively. The RDFs were computed using a bin width of 0.02 Å. Results from SET_A are shown in *blue* and results for SET_B are shown in *red*. Due to the symmetry of the interfacial slab, the computed $g_{FO}(r)$ and $g_{FH}(r)$ are expected to converge to 0.5 for SET_B.

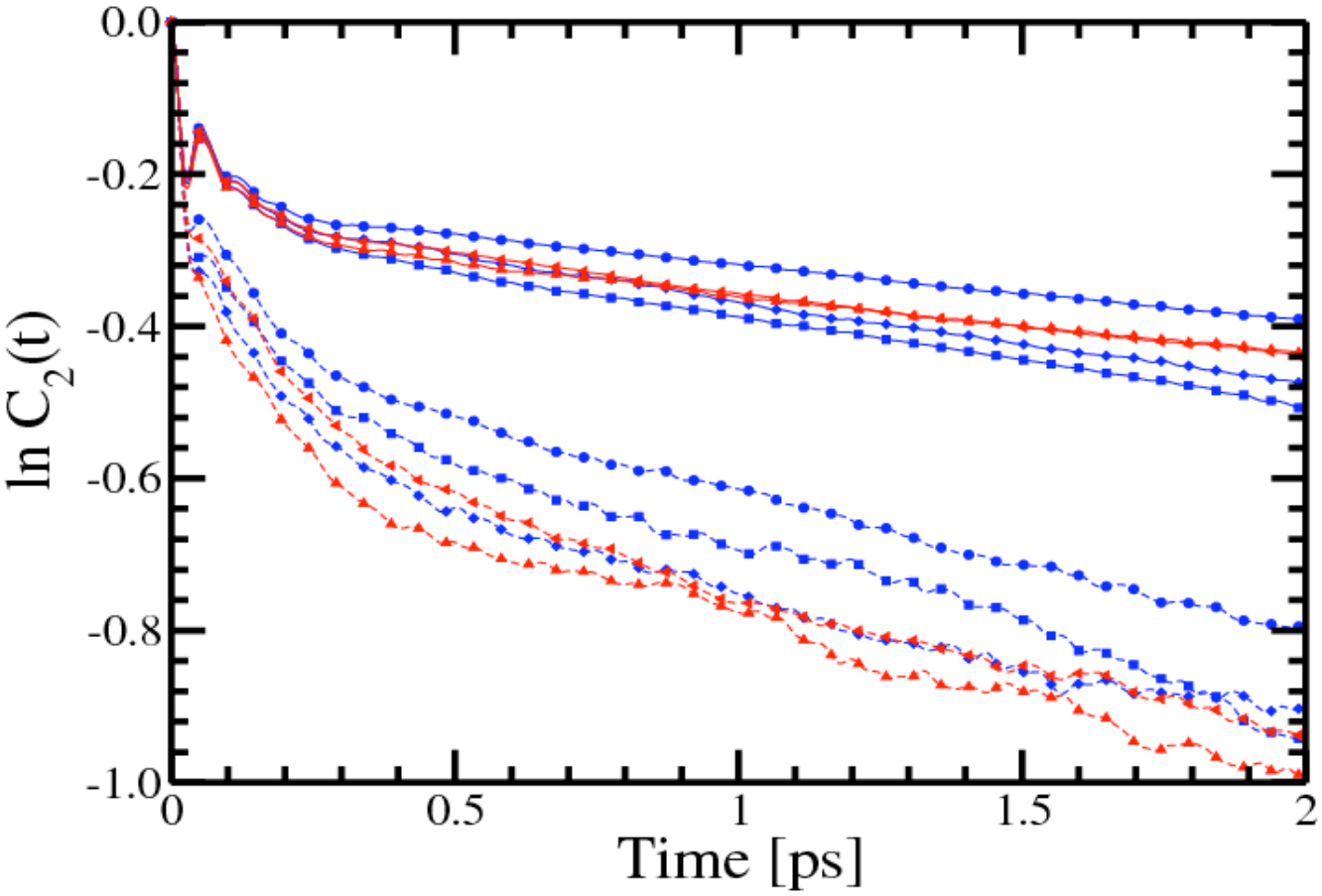

Figure 3. Second order rotational correlation times, $C_2(t)$, for water in the bulk region and at the surface. Results from SET_A are shown in *blue* and results for SET_B are shown in *red*. Each water slab has been partition into bulk and surface region which are shown using *solid* and *dashed* lines respectively.

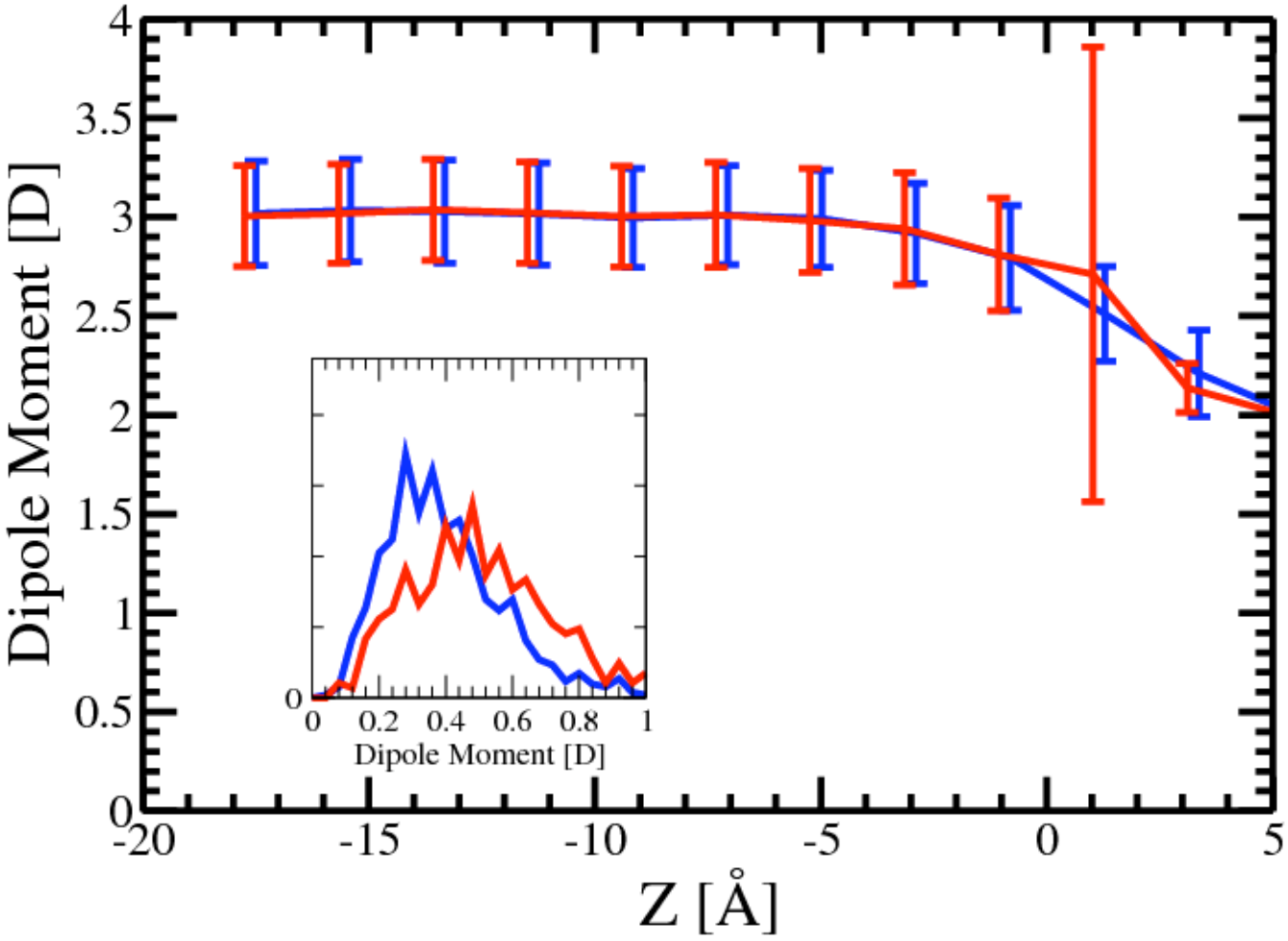

Figure 4. Molecular dipole moments for water and standard deviation as a function of slab depth. Results from SET_A are shown in *blue* and results for SET_B are shown in *red*. The interfaces are shifted so that the GDS is located at 0.0 Å. The distributions of dipole moments for fluoride are shown in the inset.

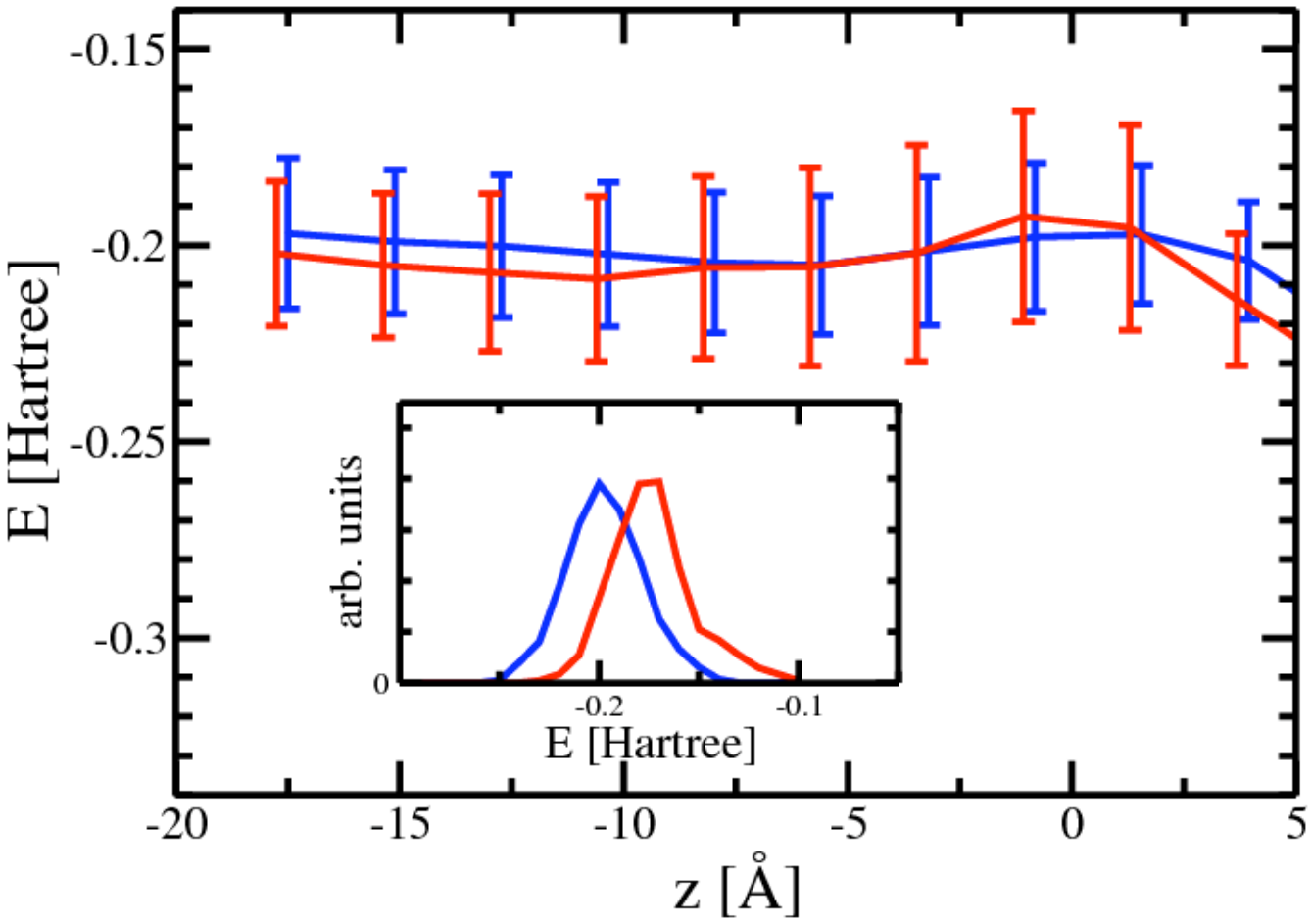

Figure 5. Effective highest occupied molecular orbital (HOMO) energies for individual water molecules and standard deviation are plotted as a function of interfacial depth. Results from SET_A are shown in *blue* and results for SET_B are shown in *red*. The HOMO energy distributions for fluoride are shown in the inset.